International Journal of Scientific Research in Science and Technology
Print ISSN: 2395-6011 | Online ISSN: 2395-602X (www.ijsrst.com)
doi : https://doi.org/10.32628/IJSRST

Design and Analysis of Multiport DC-AC Converter with DPPC for BESS Integrated PV Systems by using FLC

C.Manoj[1], M.Murali[2]
M.Tech Student[1], Associate Professor[2]
[1&2]department of EEE-Vemu Institute of Technology, P.Kothakota, Andhara Pradesh, India

Article Info
Volume 9, Issue 6
Page Number : 610-621

Publication Issue
November-December-2022

Article History
Accepted : 15 Dec 2022
Published : 30 Dec 2022

ABSTRACT

In this research work, design and analysis of BESS multiport DC-AC converter with DPPC Integrated by using FLC is implemented. The unavailability of power supply from solar PV is not uniform throughout the day. So, a battery is integrated with Solar PV. The obtained dc power from the integrated system needs to supply to the loads as well as to the grids. But the loads needs AC supply. So, a multiport ac-dc converter along with differential power processor is employed. The pulses to the MPC is given by Modified Space Vector Pulse Width Modulation Technique (SVPWM) that takes use of fluctuations in solar and battery voltage. In this project mainly, the control of active power flow is attained. In the controlling topology of MPC, PI controller is implemented to regulate the reference voltage by giving current and reference currents as inputs. But by implementing of PI controller will have less speed response of the system and high harmonic distortions. In order to overcome these issues, this paper proposes a novel controlling topology named Fuzzy Logic Controller (FLC). This will enhances the speed response of the system by maintaining good power quality. The evaluation of this system is considered in two cases namely constant irradiation and variable irradiation by using Matlab/Simulink 2018a Software.

Keywords: Solar PV, Multiport Converter, Battery, Differential Power processing Converter, PI controller, Fuzzy Logic Controller, Modified SVPWM Technique.

I. INTRODUCTION

Photovoltaic (PV) systems are widely used in daily life as a result of the sustainability of solar energy and the resulting decrease in its material cost. The use of photovoltaic (PV) energy installations is expanding quickly, both for home energy systems and substantial utility power plants [1]. A sizeable portion of this field's utilizing battery energy storage (BESS)

Technologies is the subject of study to get around solar PV power's intermittent nature. In order to integrate PV and BESS, power electronic devices perform a number of tasks, such as ac-dc conversion, Maximum power point tracking (MPPT) of the PV–

BESS management [2]. Traditional PV power electronics designs are used by grid-tied PV inverter systems to include a battery ESS [3]. One of these topologies uses a bidirectional system associated DC-AC inverter with a DC converter to further develop battery voltage; the other utilizes a unidirectional single or cascaded PV DC coupled to a bidirectional DC converter and a shared charge controller DC bus. - c) In-line integration, which entails directly coupling a battery to a common DC bus; - d) AC-series integration, which consists of integrating a bidirectional modular DC-AC converter component into an AC string [5]-[6]. As a result, Power transfer between the ports is accomplished using a three-port DC/DC converter system (TPCS). It basically functions in three different ways: the DO (dual output) mode is one of them. 2) Dual-input mode (DI). This mode is used at the point when the result force of the PV board is higher than the result power of the load (PPv>PLd). When a PV panel's output is insufficient to fulfil the demand for the load (PPV, however, have poor device utilization, low power density, low efficiency, and a high cost) (PPV, however, have poor using low-power density technology, inefficiency, and high cost), [7-8]. Solar power systems are known as differential power processing (DPP). On the other hand, [9]–[10] earlier provided the core PV DPP idea. In order to achieve DPP and minimize losses from a PV string's partial shadowing, it used battery cell balancing techniques. There are numerous approaches to balance capacitor In SVPWM applications, the three-level NPC inverter's voltages as a consequence of a superior information on the impacts of switching choices on capacitor voltages in vector space. Examples include the use of virtual SVPWM (VSVPWM), regular SVPWM, and their combination for capacitance balancing. The inverter should be able to quickly deliver the necessary voltage output while maintaining the control system's established reference vector in the ideal situation of vector control theory (Vref). It is not practicable to ensure that every required vector may be formed due to the switch restrictions of the inverter; in reality, only few vectors (27 vectors for a three-level inverter)might be created [11]-[13]. The FLC structure is built with double inputs and a single output. In order to achieve satisfactory perfection, each info variable and result are standardized in the reach of 1 to +1 during fuzzy control operation [14]-[15]. This paper is coordinated as follows: Section-I describes the literature review and introduction of this project. Section-II demonstrates the system's description. Section-III depicts about the controlling topology and modulation schemes. Section-IV depicts about the comparison of conventional proposed simulation results. Section-V ends with conclusion of this research work.

II. DESCRIPTION OF THE SYSTEM

The standard cure compared in this investigation is the conventional as depicted in Fig. 1. The DC connection and PV are connected directly (b).Despite a number of limitations on the PV string's voltage, this system is extremely effective, reasonably priced, and has a wide range of practical applications. In Fig. 1, a DC-DC converter can be seen. Control active power and guarantee voltage matching between the PV and batteries by using 1. (b). the dc-dc converter must, of course, regulate the overall electricity flowing actively through the battery. It's referred to as a full-power DC converter (FPC). Using this usual technique, the suggested configuration is created in two steps.

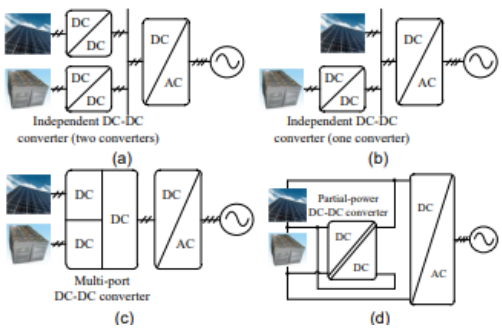

Fig. 1. PV system with integrated ESS dc-coupled batteries

1) The front-end dc converter's size has diminished to build proficiency and decline the quantity of force conversion stages. Another dc port that is directly related with the battery has moreover been worked for the dc-ac stage. The MPC design was developed to function with batteries, PV, and an AC grid, as illustrated in Fig. 2. (a). The dc-ac converter is referred to as the MPC in light of the fact that There are three ports (two dc and one ac)that are while related with the PV, battery, and ac affiliation.
2) As illustrated in Fig. 2, the battery's management and regulation techniques continually in a phase-stage MPC, limit the battery's ability to control power. A DPPC is connected between two batteries to assist the power of the dc ports regulation range (b). By assuming that P is the battery's whole active power transmission is comprised from of P1, which the MPC directly exchanges with; the dc-dc converter simply assesses the total active power. The power differential between P and P1. The DPPC is the name given to the DC-DC converter as a result.

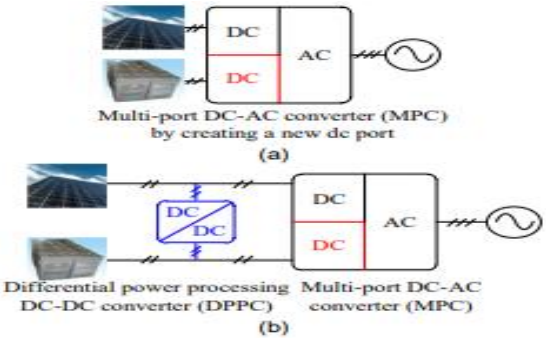

Fig. 2. The proposed architecture for a battery-ESS integrated PV system

The proposed configuration's Most of the dynamic power between the PV, batteries, and ac network may be regulated by the MPC, with only a small portion of active power requiring processing by the DPPC. The suggested configuration's fundamental functioning and active power flow are shown in Figure 4. As illustrated in Fig. 4, Only the MPC is activated to perform when the PV power fluctuates within a certain range, the dynamic power guidance of the PV and battery, preventing the DPPC from being activated (a).All active power is transported in this scenario (Case I) through a solitary high-efficiency power conversion step. The DPPC takes over and manages the differential power that the MPC is unable to control when the PV power fluctuation rises over a specific level. The DPPC only processes a small part of the power, hence it is inexpensive and has a low power rating. A sufficient amount of PV energy will utilise the DPPC in the vehicle to charge the battery event of very high PV power (Case II), according to Fig. There will be some electricity transmitted from the battery to the ac grid via the DPPC in Case III, which has extremely low or even no PV power, as illustrated in Figure 4(b). 4(c).

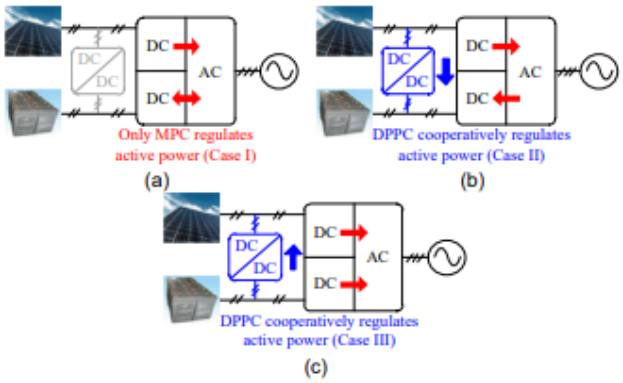

Fig. 3. The suggested configuration's fundamental functioning and active power flow are as follows: Case I, II and III

As shown in Fig. 1, the conventional The MPC architecture was heavily influenced by three-level converters. The traditional three-level converter's voltage-dividing capacitor is split off and utilised whereas the original dc connection is employed as one dc port that communicates with PV, as a new dc port that interfaces utilising the battery In this work, one MPC topology make a neutral-point clamping three-level converter (NPC),although the same method might be used to build others. In MPCs, many three-level topologies are employed. Two topologies

are the split-source The Z-source/qZ-source topology and the Z-source/qZ-source topology are two typical methodologies having two possible DC ports from which the MPC can be formed. The three-level topologies were selected for this work because they are more extensively utilised in real-world applications and are easier to understand. In Fig. 5, power flow control by correctly managing the switches S1x, S2x, S3x, and S4x (where x=a, b, c), a connection between the PV, battery, and ac grid may be made.

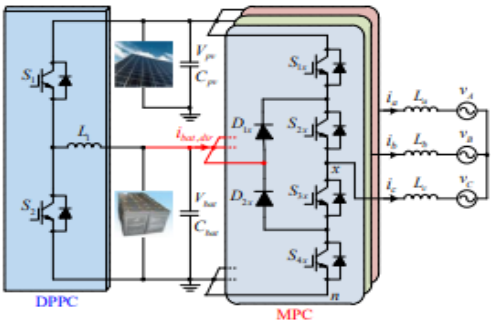

Fig. 4. MPC and DPPC topologies.

When the battery and PV voltages fluctuate, There is not always centre point voltage balance (In other words, the battery voltage does not always match the PV voltage) the control and modulation techniques of the MPC would change significantly as a result. Battery power flow in both directions necessitates the usage of bidirectional dc-dc converters is DPPC design. The system functioning in this study is shown using simple bidirectional DC-DC converter with buck/boost.According to Fig. 5, the battery and PV sources' grounds are connected to the same place, proving that the suggested design is not isolated. Additionally, the suggested design is contrasted with existing non-isolated options.

MODULATION SCHEMES AND PROPOSED CONTROLLING TOPOLOGY:

A. Controlling Topology of the System:

The suggested arrangement aims to produce high-efficiency electricity from battery and PV. The control logic should be the following in order to achieve this: (1) The single-stage MPC is preferred for regulating the Active power of batteries and PV within the MPC's power control capabilities; and (2) The DPPC is solely included in power regulation to supplement the MPC's power control skills. The implementation of active power regulation in the MPC may be likened to the voltage balancing technique used by three-level converters since the MPC design is developed from the conventional three-level converter. As is widely known, the SVPWM algorithm's positive to negative small vector ratio is always adjusted in order to ensure three-level converter voltage balance. Actually, the steps to achieve voltage balancing and the two capacitors' active power regulation is the same. This indicates that power management of the PV and batteries for the MPC may also be controlled using the modulation technique's positive-to-negative small vector ratio. The block diagram for the suggested power control approach is shown in Figure 6. The grid current that was injected is regulated using the standard P/Q control, as stated. The injected ac grid current is regulated using the standard P/Q control, as indicated. The switching signal S1 is created when k is compared to a triangle carrier with a range of -1 to 0, while the switching signal S2 is produced when k is compared to a triangular carrier with a range of 1 to 2. The system works in several scenarios with different values of k that correspond to Fig. 4.

(1) Case I: When 0k1, kc=k, both S1 and S2 are turned off. By altering the control parameter kc, the MPC alone controls the PV and battery's active power in this scenario, leaving the DPPC dormant.

(2) Case II: The control parameter kc is set to 0 when k = 0.That is, the MPC's capacity to manage power has reached one of its limits, and to accomplish PV and battery power management, more is still required. The switch S1 then begins to turn on, and The DPPC performs buck conversion.

(3) Case III: The control boundary kc is set to 1 when k outperforms 1, showing that the MPC's power

control limit has reached the other limit. When the switch S2 is turned on, the DPPC then functions as a boost converter.

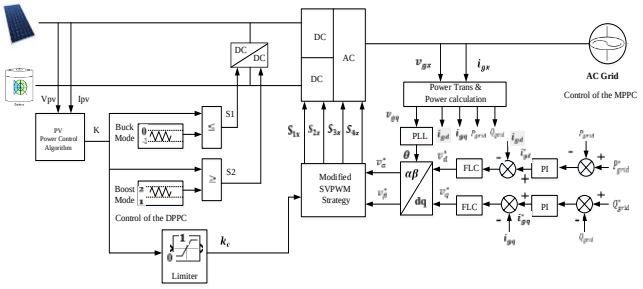

Fig. 5. Control strategy for proposed system.

B. MODIFIED SVPWM TECHNIQUE:

The MPC implements a modified SVPWM method to provide dynamic management of solar and batteries. The switching operation establishes Sx (x=a, b, c), the halfway voltage is shown by the switching variable. point of each Switching-leg vxn. When S1x and S2x activate, Sx is defined as h and vxn=Vpv and S3x and S4x deactivate. vxn=Vbat when S2x and S3x activate and S1x and S4x deactivate, and Sx is specified as l. When S3x and S4x activate and S1x and S2x deactivate, vxn equals zero and Sx equals zero. The switching states are produced by combining the switching variables of three phases (Sa, Sb, Sc). Figure 1 shows the MPC's voltage space vector diagram 7 in accordance with definition.The below figure shows vector diagram of MPC and is consists of 6 sectors

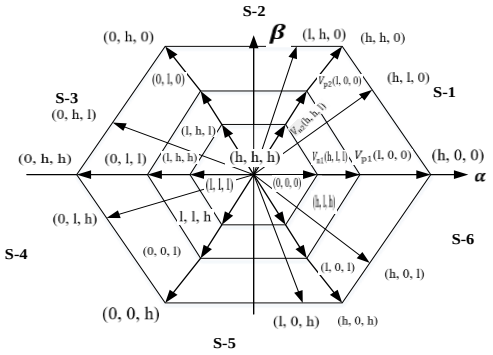

namely S-1,S-2, S-3, S-4, S-5, S-6.

Fig. 6. Vector diagram of the MPC.

All of the voltage vectors vary as h and l change since the PV and battery voltages are both variable. Except when l=h/2positive small vectors, as seen by the red strong line and negative little vectors. (As is seen by the blue solid line) cease to converge. The complete dispersion of the space vector graph is consequently imbalanced. As noted earlier, the MPC may actively control power by changing the proportion of moment positive and negative vectors. Two sets of positive and negative little vectors S-7 are available in every area, as displayed in Fig. 1. One sets of little vectors in Area I is comprised of the positive little vector Vp1(l,0,0) and the negative little vector Vn1(h,l,l), and the other pair is made up of Vp2(l,l,0) and Vn2(h,l,l) (h,h,l). Two virtual voltage vectors, Vvir1 and Vvir2, are created to circumvent this issue, and their formulae are shown below. This is due to Fig. 1's positive and negative vectors.

$$\begin{cases} \boldsymbol{V_{vir1} = k_c V_{p1} + (1 - k_c) V_{n1}} \\ \boldsymbol{V_{vir2} = k_c V_{p2} + (1 - k_c) V_{n2}} \end{cases} \quad \textbf{(1)}$$

The extent of the positive and negative tiny vectors 6 are coordinated using the control border kc, as shown in Fig. 1.

Vvir1 is located between Vp1 and Vn1 because the span of kc is 0kc1, and Vvir2 is located between Vp2 and Vn2. The six sub-sectors of Sector I are identified by the letters S1S6, and they are essentially divided the centre vector and the zero vector (l, l, l) are split into two groups by the green barrier. (l, l, l) (h, l, 0).It satisfies that below the blue boundary.

$$\boldsymbol{V_\beta \le \sqrt{3 v_r} \, . V_\alpha / (2 - v_r)} \quad \textbf{(2)}$$

Where the reference voltage vector's frame coordinates are V and V, and vr=l/h. Vref The virtual voltage vector Vvir1 is used in this region for S1S3's sub-sector division, which is assessed by

$$\textbf{Subsector} = \begin{cases} \textbf{S1 if } V_\alpha < \frac{(2k_c+3v_r-4v_rk_c-2).V_\beta}{\sqrt{3}v_r} + \frac{2(2v_rk_c+1-k_c-v_r)}{\sqrt{3}} \\ \textbf{S2 else if } V_\alpha > \frac{(2k_c+v_r-4v_rk_c).V_\beta}{\sqrt{3}v_r} + \frac{2(2v_rk_c+1-k_c-v_r)}{\sqrt{3}} \\ \textbf{S3 otherwise} \end{cases}$$

(3)

ΔIn the sub-sectors S1S3, Vvir1 is constantly utilized for reference vector combination, and kc has the capacity to control the active power flow.

It fulfils that above the blue border.

$$V_\beta > \sqrt{3v_r}\,.V_\alpha/(2-v_r)$$

(4)

Here, S4S6 sub-sector division and vector combination are done using the virtual voltage vector Vvir2. For these sub-areas, the option is

$$\textbf{Subsector} = \begin{cases} \textbf{S4 if } V_\alpha < \frac{2v_rk_c+v_r-k_c-1}{\sqrt{3}\,(2v_rk_c+1-k_c-v_r)}V_\beta + \frac{2(1-v_r)}{\sqrt{3}} \\ \textbf{S5 else if } V_\beta > \frac{\sqrt{3}(1-2v_r)(k_c-1)}{1+k_c-2v_rk_c}V_\alpha + \frac{2(1-v_r)(1+2v_rk_c-k_c-v_r)}{1+k_c-2v_rk_c} \\ \textbf{S6 otherwise} \end{cases}$$

(5)

The sub-sectors S1S6 can be uniquely determined by combining Equations (2) and (3), and (4) and (5). Following sub-sector division, the three closest vectors, V0, V1, and V2, in each sub-sector may be combined to create the reference vector Vref, also, the abide time not entirely set in stone by tackling the accompanying capability.

$$\begin{cases} V_\alpha T_s = V_{0\alpha}T_0 + V_{1\alpha}T_1 + V_{2\alpha}T_2 \\ V_\beta T_s = V_{0\beta}T_0 + V_{1\beta}T_1 + V_{2\beta}T_2 \\ T_s = T_0 + T_1 + T_2 \end{cases}$$

(6)

The frame's voltage vector has coordinates VI and VI (i=0, 1, 2), where Ts is the switching period and Ti is the period of action. Specifically, the tiny vectors Vp1 with kcTi action time and Vn1 with (1-kc) Ti action time may realize the virtual voltage vectors Vvir1 and Vvir2 once the function (6) has been solved. The described step-by-step technique for establishing virtual voltage vectors, sub-sector division, selecting voltage vectors, computing dwell periods, and organizing switching sequences, as illustrated in Table I, may be utilised to implement the enhanced SVPWM approach.

TABLE I SEQUENCE OF SWITCHING IN EACH SUB-SECTOR

Sub-sector	Switching sequences						
	$0.5k_cT_0$	$0.5T_1$	$0.5T_2$	$(1-k_c)T_0$	$0.5T_2$	$0.5T_1$	$0.5k_cT_0$
S1	(*l*,0,0)	(*l*,*l*,0)	(*l*,*l*,*l*)	(*h*,*l*,*l*)	(*l*,*l*,*l*)	(*l*,*l*,0)	(*l*,0,0)
S2	(*l*,0,0)	(*h*,0,0)	(*h*,*l*,0)	(*h*,*l*,*l*)	(*h*,*l*,0)	(*h*,0,0)	(*l*,0,0)
S3	(*l*,0,0)	(*l*,*l*,0)	(*h*,*l*,0)	(*h*,*l*,*l*)	(*h*,*l*,0)	(*l*,*l*,0)	(*l*,0,0)
S4	(*l*,*l*,0)	(*l*,*l*,*l*)	(*h*,*l*,*l*)	(*h*,*h*,*l*)	(*h*,*l*,*l*)	(*l*,*l*,*l*)	(*l*,*l*,0)
S5	(*l*,*l*,0)	(*h*,*l*,0)	(*h*,*h*,0)	(*h*,*h*,*l*)	(*h*,*h*,0)	(*h*,*l*,0)	(*l*,*l*,0)
S6	(*l*,*l*,0)	(*h*,*l*,0)	(*h*,*l*,*l*)	(*h*,*h*,*l*)	(*h*,*l*,*l*)	(*h*,*l*,0)	(*l*,*l*,0)

C. FUZZY LOGIC CONTROLLER:

(FLC), which operates based on logical rules formed by input and output arguments. And also it converts crisp values to fuzzy values (analog to logical). It is implemented by using the membership functions. The FLC system mainly compresses of 4 major parts known as fuzzification (converts fuzzy sets to crisp sets), rules base, inference engine and defuzzification (crisp sets to fuzzy sets) which can be depicted in below figure.

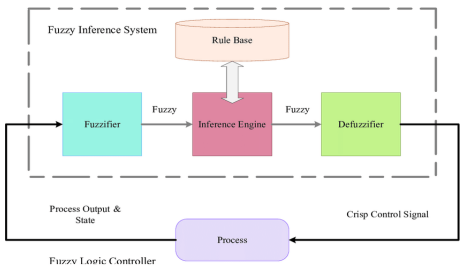

Fig 7: Schematic diagram of FLC

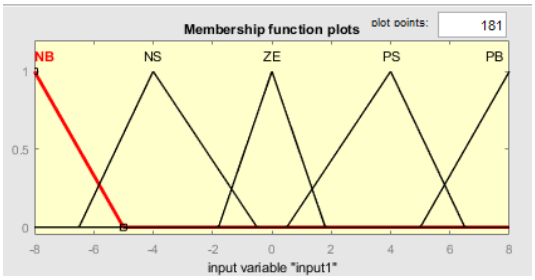

Fig 8: Input 1 (Error)

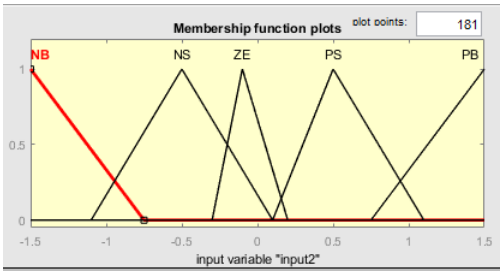

Fig 9: Input 2 (Change in Error)

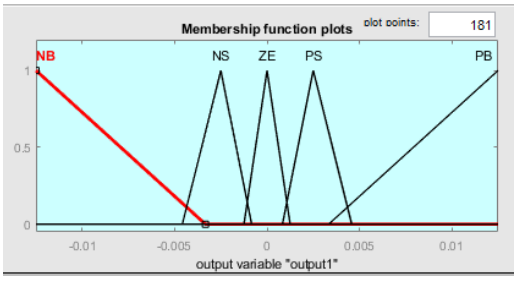

Fig 10: Output Membership function

The above figures will depicts about the FLC system configuration, inputs (e-Δe), and output membership functions.

III. SIMULATION BASED RESULTS:

This section will depicts about the simulation based results obtained in two cases namely constant irradiation and variable irradiation. This results evaluates the comparison of both conventional and proposed topologies.

A) By using PI Controller:

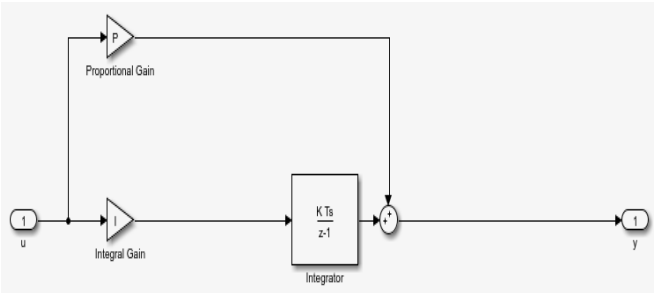

Fig 11: Topology of PI Controller

The above figure will depicts about the controlling topology of PI controller.

i) AT CONSTANT IRRADIATION:

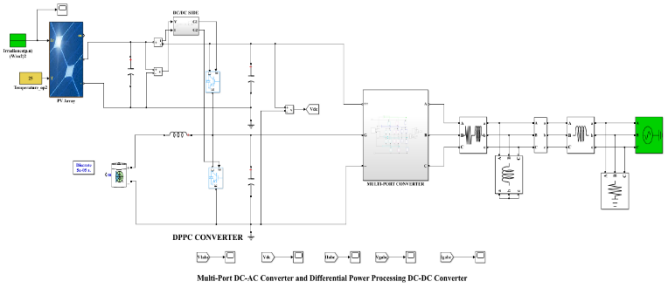

Fig 12: Schematic diagram of the system at constant Irr.

In this case, the irradiance is maintained constant at a value of 1000W/m². The controlling topology is fed with PI controller. The above figure will shows the system's Simulink model. In relation to simulation results are mentioned below.

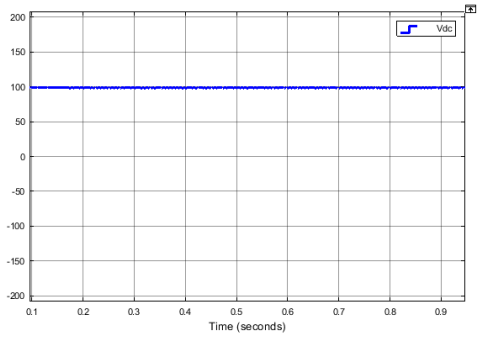

Fig 13: Vdc

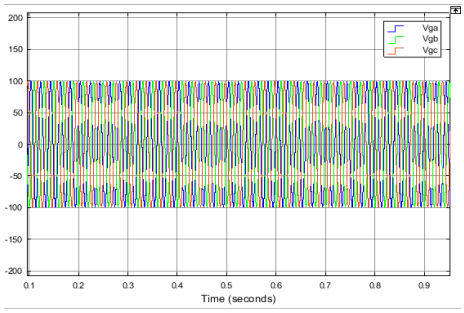

Fig 14: Vgabc

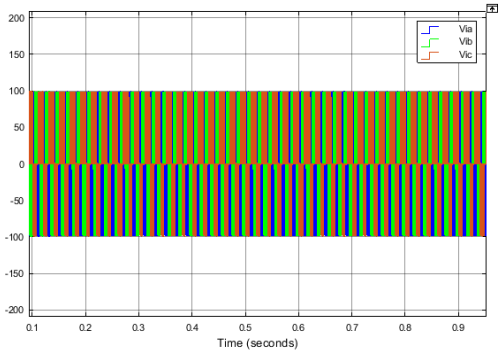

Fig 15: Viabc

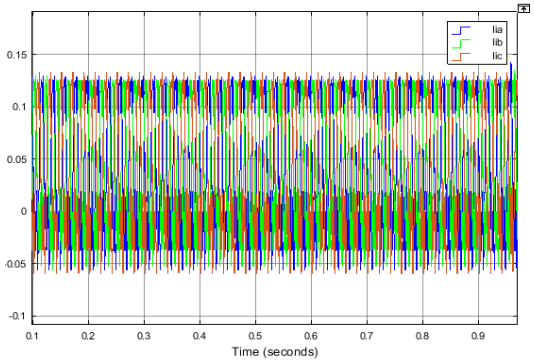

Fig 16: Iiabc

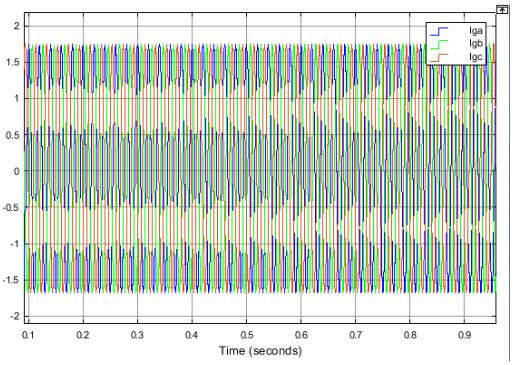

Fig 17: Igabc

The above figures will depicts about the simulation results obtained related to the inverter, grid and dc link based currents and voltages. At constant irradiation, the DC link voltage has attained constant at a value of 100V. The attained amplitude of grid voltage and current is 100V and 1.75A in sinusoidal form whereas the voltage and current values obtained in Inverter is 100V and 0.13A of amplitude.

At VARIABLE IRRADIATION:

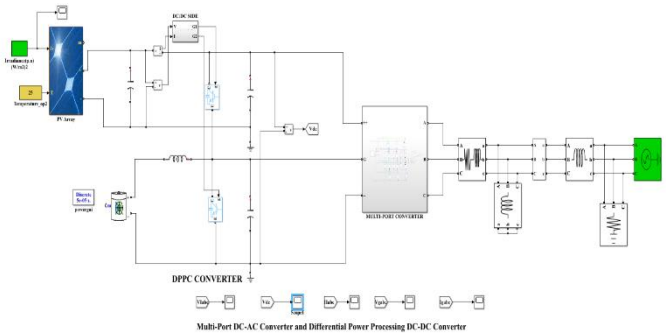

Fig 18: Schematic diagram of the system at varied irr.

In this case, the irradiance is varied at a value of 500 W/m²-1000W/m². The controlling topology is fed with PI controller. The above figure will is a representation of the system's Simulink model. As it relates simulation results are mentioned below.

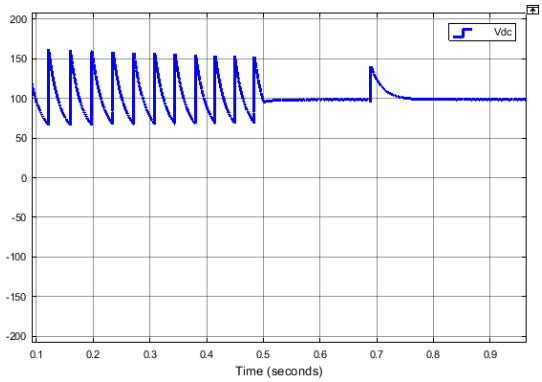

Fig 19: Vdc

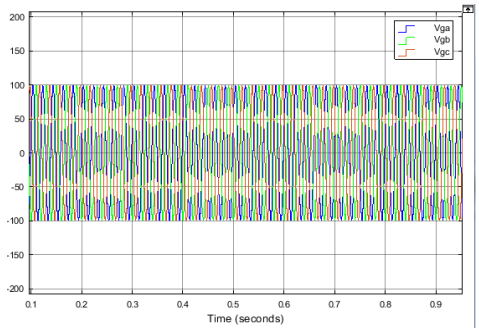

Fig 20: Vgabc

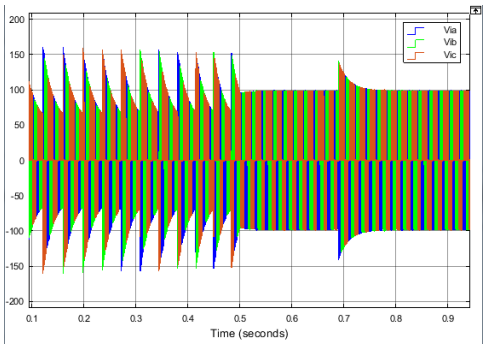

Fig 21: Viabc

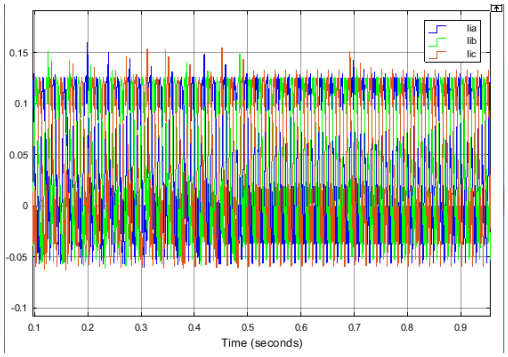

Fig 22: Iiabc

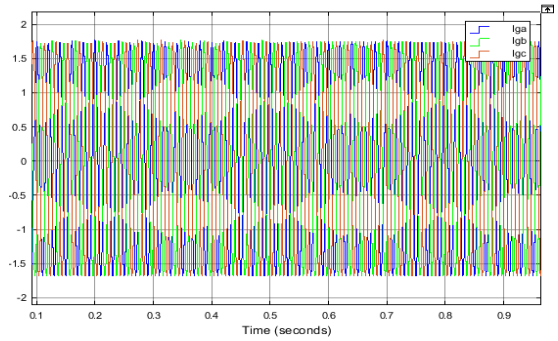

Fig 23: Igabc

The above figures will depicts about the simulation results obtained related to the inverter, grid and dc link based currents and voltages. In this case, at 500W/m² of irradiance the magnitudes of all components is high when the irradiance is increased to 1000W/m² the magnitudes are decreased and is having some harmonic distortions.

FLC BASED RESULTS:

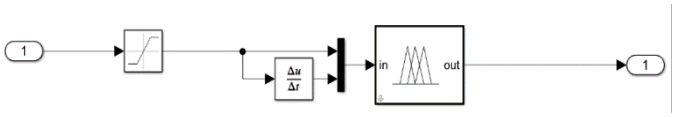

Fig 24: Schematic Diagram of FLC

The above figure will depicts the FLC schematic diagram. It is implemented in the place of PI Controller.

At Constant Irradiation:

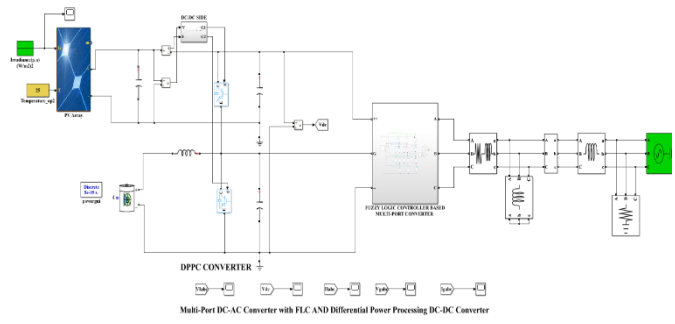

Fig 25: Schematic Diagram of the proposed system with constant irradiance

In this case, the irradiance is maintained constant at a value of 1000W/m². The controlling topology is fed with flc controller. The above figure will depicts the simulink model of the system. This related simulation results are mentioned below.

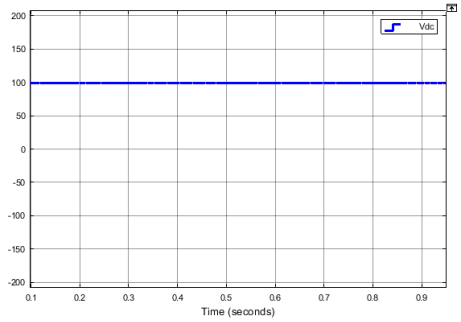

Fig 26: Vdc

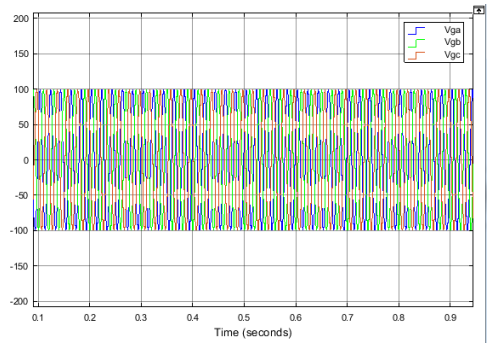

Fig 27: Vgabc

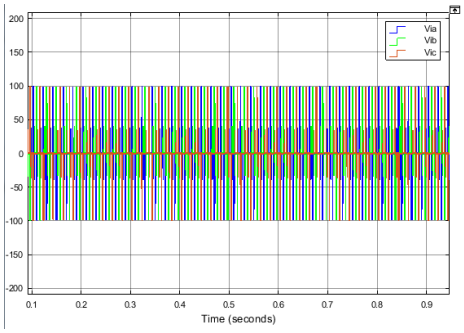

Fig 28: Viabc

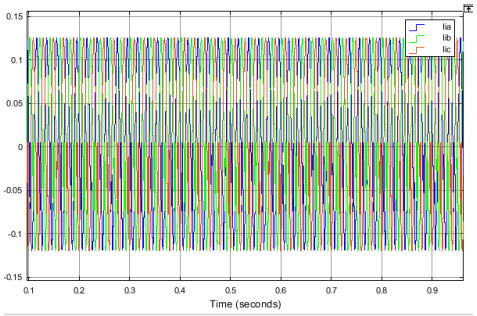

Fig 29: Iiabc

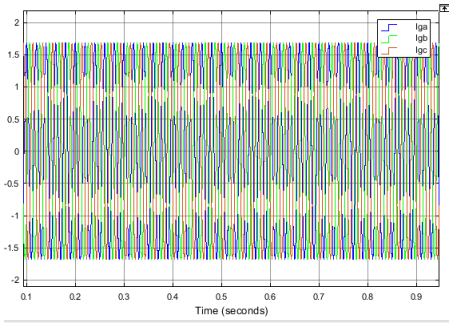

Fig 30: Igabc

The above figures will depicts about the simulation results obtained related to the inverter, grid and dc link based currents and voltages. At constant irradiation, the DC link voltage has attained constant at a value of 100V. The attained amplitude of grid voltage and current is 100V and 1.75A in sinusoidal form whereas the voltage and current values obtained in Inverter is 100V and 0.13A of amplitude. Due to employing FLC, no distortions are attained in the waveforms.

At Variable Irradiation:

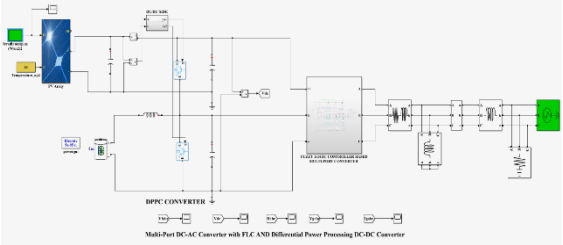

Fig 31: Schematic Diagram of proposed system with varied irradiance

In this case, the irradiance is varied at a value of 500 W/m²-1000W/m². The controlling topology is fed with FLC controller. The above figure will depicts the simulink model of the system. This related simulation results are mentioned below.

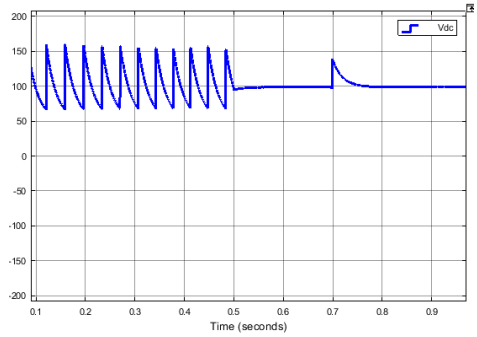

Fig 32: Vdc

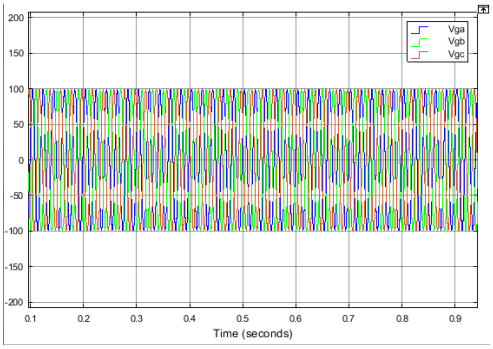

Fig 33: Vgabc

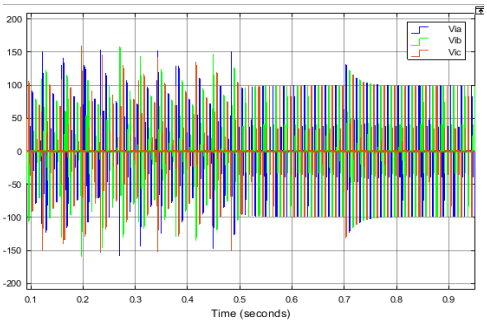

Fig 34: Viabc

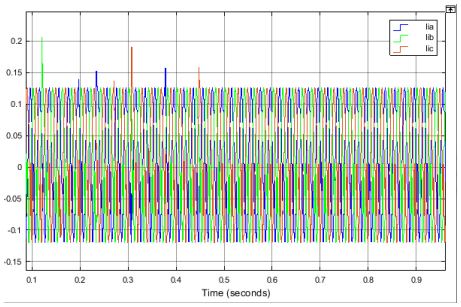

Fig 35: Iiabc

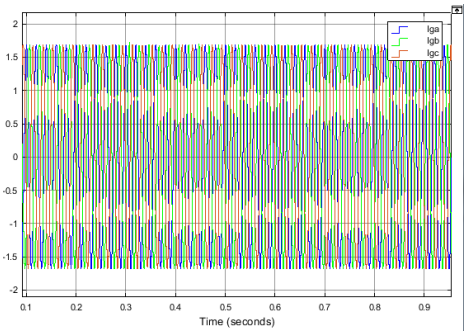

Fig 36: Igabc

The above figures will depicts about the simulation results obtained related to the inverter, grid and dc link based currents and voltages. In this case, at 500W/m² of irradiance the magnitudes of all components is high when the irradiance is increased to 1000W/m² the magnitudes are decreased. Although it has some disturbances in the waveforms due to variation in irradiance the implementation of FLC in

the circuit has attained less distortions in the waveform.

Component	THD obtained using PI Controller	THD obtained using FLC
Inverter Current obtained at Constant Irradiation	34.84%	28.90%
Inverter Current obtained at Variable irradiation THD	34.19%	28.64%

Table 2: Comparison of THD

The above table will describes about the comparison of THD in Inverter current by using PI controller and Fuzzy Logic controller. The % of THD obtained in inverter current at constant irradiation by using PI Controller is 34.84%, whereas by using FLC it is reduced to 28.90%. The % of THD obtained in inverter current at variable irradiation by using PI Controller is 34.19% whereas by using FLC it is reduced to 28.64%. By comparing these two THD values, the FLC has evaluated less THDs in inverter current and has obtained good power quality in the system when compared to the PI controller.

IV. CONCLUSION

Design and Analysis of Multiport DC-AC Converter with DPPC for BESS Integrated PV Systems by using FLC was implemented in this research work. The power supply to the loads as well as to the grid has been considered from the solar. The availability of power from the solar is not uniform throughout the day. A battery is integrated with Solar PV. The obtained power is in DC so, an MPC along with DPPC has been employed. The pulses to this converter was evaluated by using SVPWM. In the MPC controlling topology FLC has been employed due to the drawbacks occurred in the conventional PI controller. This proposed controller has evaluated the best results than the conventional controller. The speed response of the system as well as the power quality has improved in the system. The improvement of power quality can be seen clearly in the evaluated THD values. This performance analysis has been evaluated by using the Matlab/Simulink 2018a Software.

V. REFERENCES

[1]. F. Blaabjerg and D. M. Ionel, “Renewable energy devices and systems – state-of-the-art technology, research and development, challenges and future trends,” Electric Power Components and Systems, vol. 43, no. 12, pp. 1319–1328, 2015.

[2]. F. Blaabjerg and D. M. Ionel, Renewable Energy Devices and Systems with Simulations in MATLAB R and ANSYS R. CRC Press, 2017.

[3]. S. B. Kjaer, J. K. Pedersen, and F. Blaabjerg, "A review of single-phase grid-connected inverters for photovoltaic modules," IEEE Transactions on Industry Applications, vol. 41, no. 5, pp. 1292-1306, Sep. 2005

[4]. S. Kouro, J. I. Leon, D. Vinnikov, and L. G. Franquelo, "Grid-connected photovoltaic systems: An overview of recent research and emerging PV converter technology," IEEE Industrial Electronics Magazine, vol. 9, no. 1, pp. 47-61, Mar. 2015.

[5]. B. I. Rani, G. S. Ilango, and C. Nagamani, "Control strategy for power flow management in a PV system supplying DC loads," IEEE

Transactions on Industrial Electronics, vol. 60, no. 8, pp. 3185-3194, Aug. 2013.

[6]. S. J. Chiang, K. T. Chang, and C. Y. Yen, "Residential photovoltaic energy storage system," IEEE Transactions on Industrial Electronics, vol. 45, no. 3, pp. 385-394, Jun. 1998.

[7]. Sun K, Zhang L, Xing Y, Guerrero JM, "A distributed control strategy based on dc bus signalling for modular photovoltaic generation system with battery energy storage, " IEEE Trans Power Electron, vol. 26, no. 10, pp. 3032–45, 2011.

[8]. W. Jiang and B. Fahimi. "Multiport power electronic interface-Concept, modelling, design," IEEE Trans. Power Electron., vol. 26, no. 7, pp. 1890–1900, Jul. 2011.

[9]. P. S. Shenoy, K. A. Kim, B. B. Johnson, and P. T. Krein, "Differential power processing for increased energy production and reliability of photovoltaic systems," IEEE Trans. Power Electron., vol. 28, no. 6, pp. 2968–2979, 2013.

[10]. P. S. Shenoy and P. T. Krein, "System and method for optimizing solar power conversion," US Patent US 8 508 074 B2, Aug. 13, 2013.

[11]. J. Pou, J. Zaragoza, S. Ceballos, M. Saeedifard, and D. Boroyevich, "A carrier-based PWM strategy with zero-sequence voltage injection for a three-level neutral-point-clamped converter," IEEE Trans. Power Electron., vol. 27, no. 2, pp. 642–651, Feb. 2012.

[12]. J. Wei-dong, D. Shao-wu, C. Liu-chen, Y. Zhang, and Q. Zhao, "Hybrid PWM strategy of SVPWM and VSVPWM for NPC three-level voltagesource inverter," IEEE Trans. Power Electron., vol. 25, no. 10, pp. 2607–2619, Oct. 2010.

[13]. J. Zaragoza, J. Pou, S. Ceballos, E. Robles, P. Ibaez, and J. L. Villate, "A comprehensive study of a hybrid modulation technique for the neutralpoint-clamped converter," IEEE Trans. Ind. Electron., vol. 56, no. 2, pp. 294–304, Feb. 2009.

[14].]. Hannan, M.A.; Lipu, M.S.H.; Ker, P.J.; Begum, R.A.; Agelidis, V.G.; Blaabjerg, F. Power electronics contribution to renewable energy conversion addressing emission reduction: Applications, issues, and recommendations. Appl. Energy 2019, 251, 113404.

[15]. Islam, S.U.; Zeb, K.; Din, W.U.; Khan, I.; Ishfaq, M.; Hussain, A.; Busarello, T.D.C.; Kim, H.J. Design of robust fuzzy logic controller based on the levenberg marquardt algorithm and fault ride through strategies for a grid-connected PV system. Electronics 2019, 8, 429.

Cite this article as :

C. Manoj, M. Murali, "Design and Analysis of Multiport DC-AC Converter with DPPC for BESS Integrated PV Systems by using FLC", International Journal of Scientific Research in Science and Technology (IJSRST), Online ISSN : 2395-602X, Print ISSN : 2395-6011, Volume 9 Issue 6, pp. 610-621, November-December 2022.

Journal URL : https://ijsrst.com/IJSRST229699